

RADIO CONTINUUM AND H 2α RECOMBINATION LINE OBSERVATIONS OF G34.26+0.15 AND G5.89–0.39

C. A. Rodríguez-Rico,¹ L. F. Rodríguez, and Y. Gómez

Instituto de Astronomía
Universidad Nacional Autónoma de México, Campus Morelia, México

Received 2001 September 11; accepted 2001 December 21

RESUMEN

Reportamos observaciones de continuo a 8.3 GHz y de la línea de recombinación H 2α hechas con el VLA hacia las regiones de formación estelar G34.26+0.15 y G5.89–0.39. Ambas regiones tienen opacidad promedio en el continuo a 8.3 GHz que es considerable, $\tau_c \simeq 2$, y la línea H 2α puede utilizarse para estudiar las variaciones de opacidad como función de la posición. Detectamos emisión de la línea H 2α en la componente ultracompacta A en G34.26+0.15, pero no en la componente ultracompacta B. Este resultado es intrigante porque ambas componentes ultracompactas son similares en densidad de flujo en el continuo y en tamaño angular. Si bien G5.89–0.39 muestra fuertes gradientes de velocidad en la línea H 2α , éstos no pueden explicarse solamente con rotación, como se ha propuesto anteriormente.

ABSTRACT

We report VLA observations of 8.3 GHz continuum and H 2α radio recombination line towards the star forming regions G34.26+0.15 and G5.89–0.39. Both regions show considerable mean optical depth in the continuum at 8.3 GHz, $\tau_c \simeq 2$, and the H 2α line can be used to study opacity variations across the face of the nebula. We detected H 2α emission in the ultracompact component A of G34.26+0.15, but not in the ultracompact component B. This result is puzzling since both ultracompact components are similar in continuum flux density and angular size. G5.89–0.39 shows strong velocity gradients in the H 2α line, but these cannot be attributed only to rotation, as previously proposed.

Key Words: **H II REGIONS — ISM: INDIVIDUAL (G34.26+0.15, G5.89–0.39) — RADIO LINES: ISM**

1. INTRODUCTION

Compact H II regions (< 0.1 pc) are small ionized regions found around one or more young luminous OB stars deeply embedded in their parent molecular cloud. These sources are known to exhibit distinct morphologies (Wood & Churchwell 1989; Kurtz, Churchwell, & Wood 1994), possibly reflecting the conditions of the surrounding gas. The relationship between H II regions and their environment has been one of the motivations to further study the radio recombination lines (RRLs) of H II regions, in order to understand the conditions of the interstellar medium in which these massive stars are formed. RRL from compact H II regions provide a valuable

tool to study their velocity structure, which can assist in the determination of the type of H II region and can lead to possible models (Garay, Lizano, & Gómez 1994; Gaume, Fey, & Claussen 1994; Garay & Lizano 1999). In this work we analyze the velocity structure, through the RRL H 2α , toward two compact H II regions: G34.26+0.15, which exhibits a cometary-like morphology (Reid & Ho 1985), and G5.89–0.39, which exhibits a shell-like shape with bipolar lobes (Zijlstra et al. 1990; Gómez et al. 1991). Both compact H II regions are characterized by having unusually large radio recombination line widths (≥ 50 km s $^{-1}$), which are difficult to explain with thermal broadening plus turbulent motions (Garay, Reid, & Moran 1985; Afflerbach et al. 1996). These regions show OH and H 2 O maser emission, suggesting that they are young, active star forming regions.

¹National Radio Astronomy Observatory, USA.

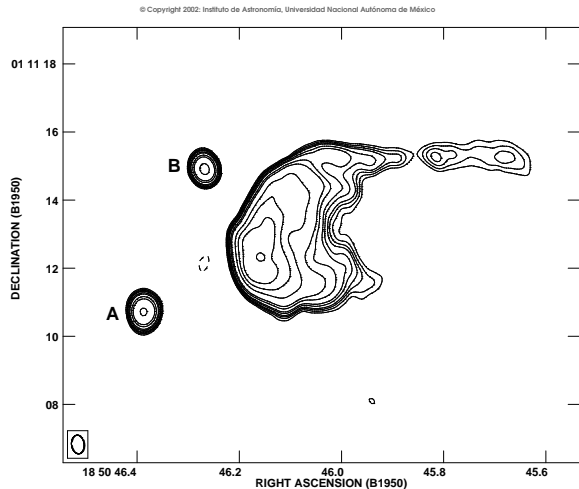


Fig. 1. VLA continuum contour map of G34.3+0.15 at 3.6 cm, made with natural weighting. Contour levels are $-3, 3, 4, 5, 6, 8, 10, 15, 20, 40, 60,$ and 80 mJy/beam. The rms noise of this map is 0.46 mJy/beam. The ultra-compact components A and B are indicated. The half power contour of the beam, $0''.55 \times 0''.37$, with $PA = 7^\circ$, is shown in the bottom left corner.

G34.26+0.15 is an H II region studied at many wavelengths, including radio continuum (Turner et al 1974; Reid & Ho 1985; Wood & Churchwell 1989), radio recombination lines (Garay et al. 1985; Garay, Rodríguez, & van Gorkom 1986; Gaume et al. 1994; Fey et al. 1994) and molecular lines (Benson & Johnston 1984; Heaton et al 1985; Anderson & Garay 1986; Gaume & Mutel 1987; Keto, Ho, & Reid 1987; Garay & Rodríguez 1990; Carral & Welch 1992; Watt & Mundy 1999; Gómez et al 2000). Radio continuum observations show a cometary ultracompact (UC) H II region with extent of $\sim 4''$, with two UC H II regions to its east, each $\sim 1''$ in angular size, and an extended ring-like H II region. The cometary region seems to be excited by one O7 ZAMS star, assuming a distance of 3.3 kpc (Kuchar & Bania 1994). $H76\alpha$ recombination line observations revealed a velocity gradient, in the north-south direction across the cometary H II region, of ~ 16 km s $^{-1}$ arcsec $^{-1}$, interpreted as ionized gas rotating perpendicularly to the symmetry axis of the cometary H II region (Garay et al. 1986; Gaume et al. 1994). The molecular gas also exhibits a velocity gradient of ~ 15 km s $^{-1}$ arcsec $^{-1}$ over ~ 0.2 pc (Carral & Welch 1992; Akeson & Carlstrom 1996; Gómez et al. 2000) but in an opposite sense to the velocity gradient of the ionized gas.

G5.89–0.39 (also known as W28 A2) has been studied extensively at radio and IR wavelengths. The radio continuum emission toward this source is

optically thick for wavelengths > 1.3 cm (Gómez et al. 1991). The H II region may be excited by at least one O6 ZAMS star, assuming a distance of 2.6 kpc (Downes et al. 1980). G5.89–0.39 has one of the most powerful and massive molecular outflows observed in the Galaxy (Harvey & Forveille 1988; Cesaroni et al. 1991; Zijlstra et al. 1990; Acord et al. 1997). The radio continuum exhibits a shell-like core with angular diameter of $\sim 4''$ and faint bipolar lobes in the northwest-southeast direction (Gómez et al. 1991). The orientation of the molecular outflow remains uncertain and it has not been possible to make a reliable comparison between the ionized and molecular outflows. However, the high velocity gas traced both by CS (Cesaroni et al. 1991) and by the H $_2$ O masers (Hofner & Churchwell 1996) suggests an orientation similar to that observed in the radio continuum bipolar lobes.

2. OBSERVATIONS

The observations were made with the Very Large Array (VLA) of the National Radio Astronomy Observatory² (NRAO) in the spectral line mode on 1991 July 09. The array was in the A configuration. We observed with one polarization and a 12.5 MHz bandwidth with 64 channels having a frequency separation of 195.3 kHz (7.0 km s $^{-1}$). The spectral window was centered at a frequency approximately intermediate between the H92 α and He92 α recombination lines. The angular resolution was $\sim 0''.4$ for images made with natural weighting. The flux density scale was determined by observing 1328+307, for which we assumed a flux density of 5.25 Jy at 3.6 cm. The phase calibrator was 1749+096, for which we derive a flux density of 1.71 ± 0.01 Jy. The bandpass calibration was made using the calibrator 1226+023. The observations of G5.89–0.39 were made at a v_{LSR} of 10.0 km s $^{-1}$, while those of G34.26+0.15 were made at a v_{LSR} of 53.0 km s $^{-1}$. All data were edited and calibrated following standard procedures for line data and images were made using the NRAO software AIPS. The spectral data were further calibrated by applying the solution obtained from a self-calibration on the continuum channel (which contains the average of the central 75% of the bandpass).

3. RESULTS AND DISCUSSION

3.1. G34.26+0.15

A 3.6 cm map of this region made from the continuum channel is shown in Figure 1. The well known

²The National Radio Astronomy Observatory is a facility of the National Science Foundation operated under cooperative agreement by Associated Universities, Inc.

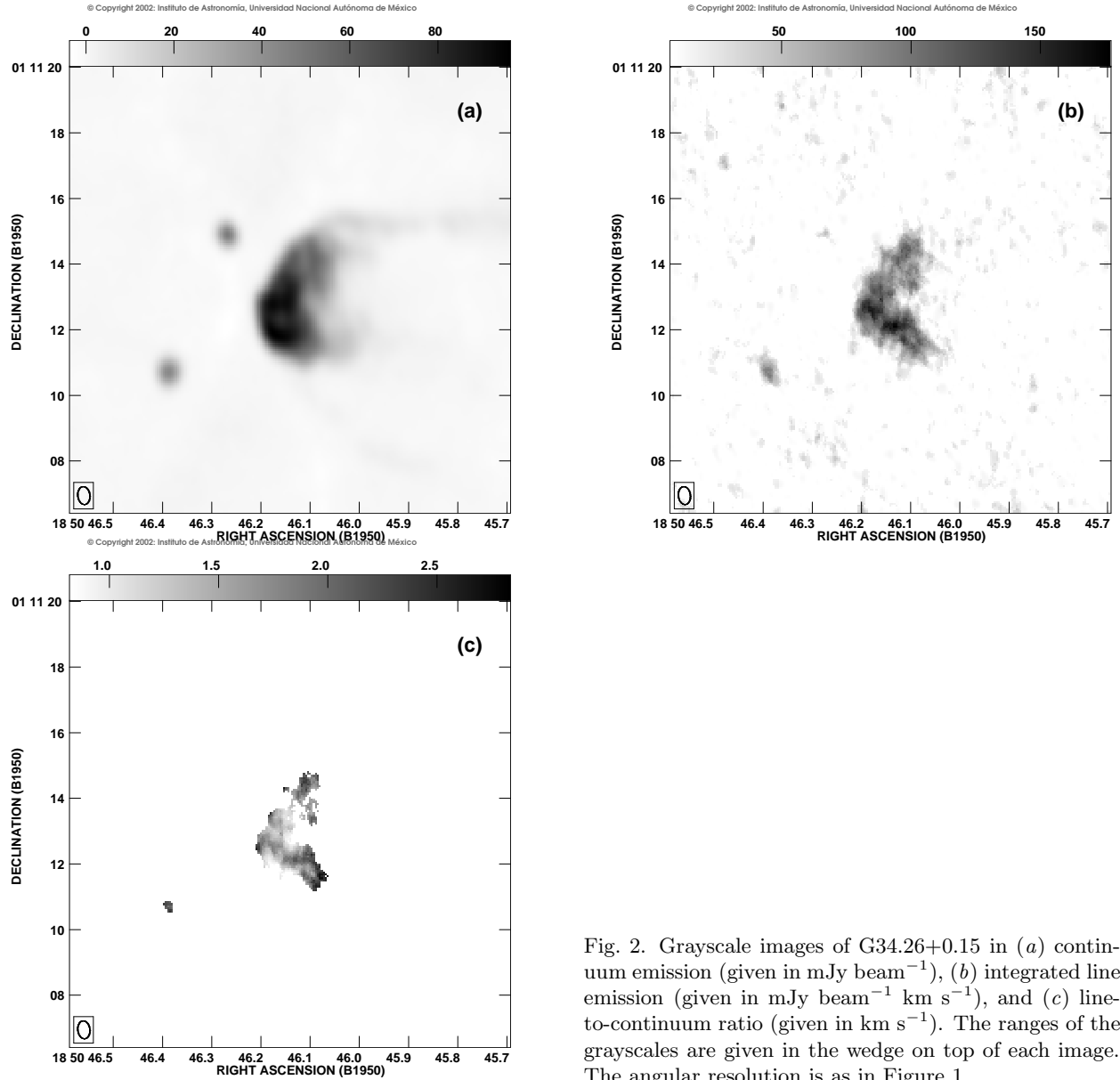


Fig. 2. Grayscale images of G34.26+0.15 in (a) continuum emission (given in mJy beam^{-1}), (b) integrated line emission (given in $\text{mJy beam}^{-1} \text{ km s}^{-1}$), and (c) line-to-continuum ratio (given in km s^{-1}). The ranges of the grayscales are given in the wedge on top of each image. The angular resolution is as in Figure 1.

cometary morphology of the H II region is clearly evident, with the “tail” to the west and the “head” to the east. We can also observe the ultracompact components A and B (Reid & Ho 1985) to the east of the “head”. The 3.6 cm total flux density of G34.26+0.15 is 2.36 ± 0.01 Jy. We do not expect to miss significant amounts of flux density in our maps since for the A configuration at 3.6 cm the largest angular scale detectable is $\sim 7''$, while most of the flux from the source originates at comparable or smaller angular scales. Since at higher frequencies the total flux density of this source reaches ~ 5 Jy, we corroborate the conclusion of Garay et al. (1986) that the source is optically thick below ~ 10 GHz. From

the observed flux densities at several frequencies, we estimate a 3.6 cm average optical depth of ~ 1.7 in the continuum.

For the ultracompact components A and B we obtain total flux densities of 84 ± 1 mJy and 72 ± 1 mJy, respectively. The deconvolved angular diameters are $0''.4$ and $0''.3$, for components A and B, respectively. The observed flux densities and angular diameters imply brightness temperatures of about 10^4 K for components A and B, suggesting considerable optical depth in the continuum. From the flux densities reported for sources A and B at 4.8 GHz (33.5 and 20.5 mJy; Wood & Churchwell 1989), 8.3 GHz (84 and 72 mJy; this paper), and 14.7 GHz (140 and 110

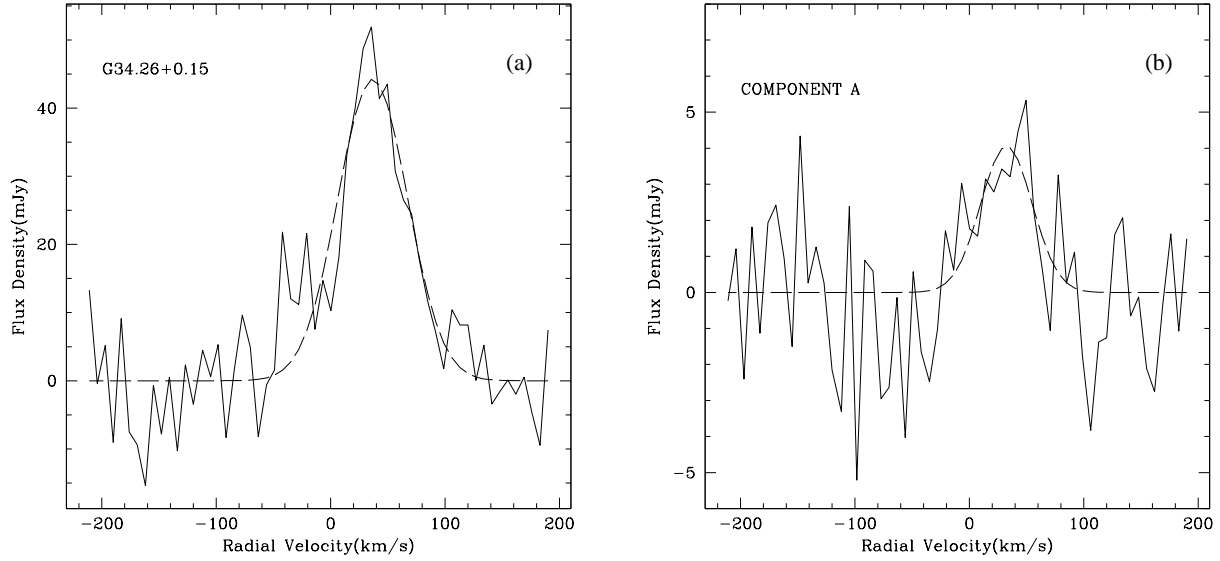


Fig. 3. (a) H92 α spectra from the cometary H II region G34.26+0.15 and (b) from the compact component A. The dashed line indicates the least-squares fit to the data.

mJy; Garay et al. 1986) we estimate average optical depths at 8.3 GHz of ~ 2 for both components.

Despite the evidence of significant optical depth in the continuum, we clearly detected H92 α emission toward the cometary region and toward component A. In Figure 2, we show the continuum emission, the integrated line emission, and the line-to-continuum ratio for the region.

Assuming that the line and continuum have the same excitation temperature, for a given radial velocity we have that

$$\frac{S_\ell(v)}{S_c} = \frac{\{1 - e^{-[\tau_c + \tau_\ell(v)]}\} - (1 - e^{-\tau_c})}{(1 - e^{-\tau_c})}. \quad (1)$$

Now, if we assume that the line (but not necessarily the continuum) is optically thin, the integrated line-to-continuum ratio will be given by

$$\frac{\int S_\ell dv}{S_c} = \frac{\int \tau_\ell dv}{(e^{\tau_c} - 1)}. \quad (2)$$

Adopting an electron temperature of 7500 K (Garay et al. 1986) and ignoring the effect of ionized helium, we find that for the H92 α line

$$\int \tau_\ell dv = 2.7\tau_c. \quad (3)$$

Then, the observed integrated line-to-continuum ratio can be used to estimate the continuum opacity

using

$$\frac{\int S_\ell dv}{S_c} = \frac{2.7\tau_c}{(e^{\tau_c} - 1)}. \quad (4)$$

This equation implies that integrated line-to-continuum ratios of $\sim 2.7 \text{ km s}^{-1}$ are expected from optically thin regions, while integrated line-to-continuum ratios of $\sim 0.9 \text{ km s}^{-1}$ will be observed in regions where $\tau_c \simeq 2$.

In Figure 2(c) we can see that the edges of the cometary H II region have low optical depths, while the center of the region reaches optical depths of 1 to 2.

We also detect H92 α line emission from the ultra-compact component A, but not from B. The detection of H92 α in component A is unexpected, given that (as derived above) the continuum optical depth of the region at 8.3 GHz is ~ 2 . Indeed, something seems to be enhancing the line emission, because the integrated line-to-continuum ratio for a continuum optical depth of ~ 2 under LTE conditions is about 0.9 km s^{-1} , while we observe $\sim 2.2 \text{ km s}^{-1}$. On the other hand, the non detection of component B seems to imply $\tau_c \geq 2$, in agreement with the continuum optical depth derived from the observed continuum flux densities. Given the similarity in angular size and continuum flux densities of components A and B, it is not easy to account for the difference in H92 α emission.

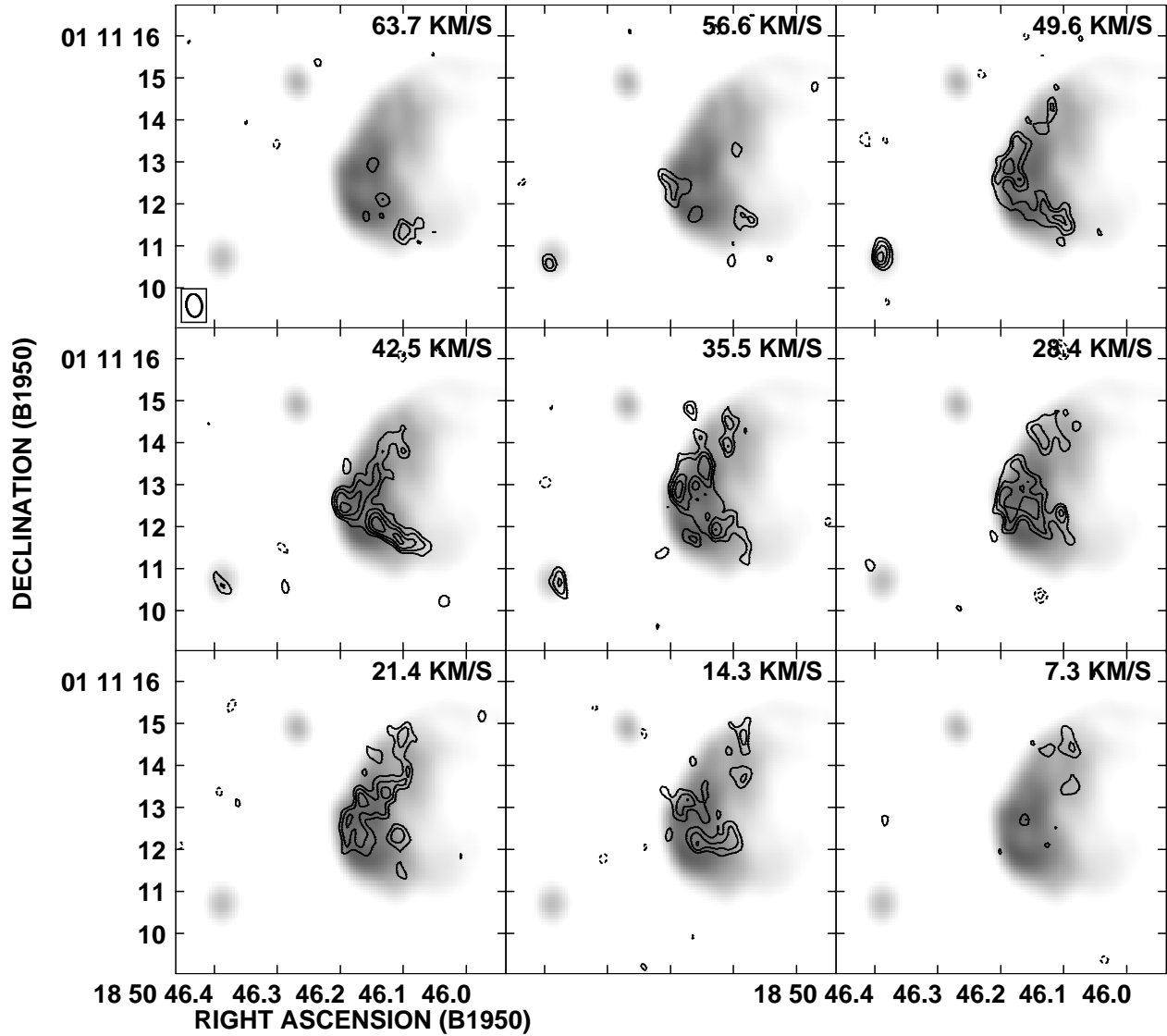


Fig. 4. Channel images of the H92 α emission from G34.26+0.15. Contours are $-3, 3, 4, 5, 6, 7,$ and 8 times $0.57 \text{ mJy beam}^{-1}$. The LSR radial velocity is shown in the top right side of each map. The continuum emission above 6 mJy beam^{-1} is shown in grayscale.

However, it should be noted that despite their similarity in the radio continuum, the ultracompact components A and B are quite different in other continuum and line tracers. Campbell et al. (2000) clearly detected component A in the mid-IR, but failed to detect component B. This result suggests that component B is probably a younger, more deeply embedded source than component A. This suggestion is supported by the image of the OH masers in the region, which shows several features associated with component B, but none with component A (Gaume & Mutel 1987; Zheng, Reid, & Moran 2000). Finally, Hatchell, Fuller, & Mil-

lar (2001) suggest that component B is the driving source of a massive outflow seen in SiO. It is well known that the driving sources of molecular outflows are generally deeply embedded in surrounding gas.

In Figure 3 we show the spatially integrated H92 α spectra from the cometary and from component A. The peak flux density, full width at half maximum, and radial LSR velocity are $44.2 \pm 3.1 \text{ mJy}$, $71.7 \pm 5.8 \text{ km s}^{-1}$, and $36.8 \pm 2.4 \text{ km s}^{-1}$ for the cometary region, and $4.1 \pm 1.0 \text{ mJy}$, $53.0 \pm 15.1 \text{ km s}^{-1}$, and $32.5 \pm 6.4 \text{ km s}^{-1}$ for component A. The line width observed toward component A, although large for an HII region, seems to disagree

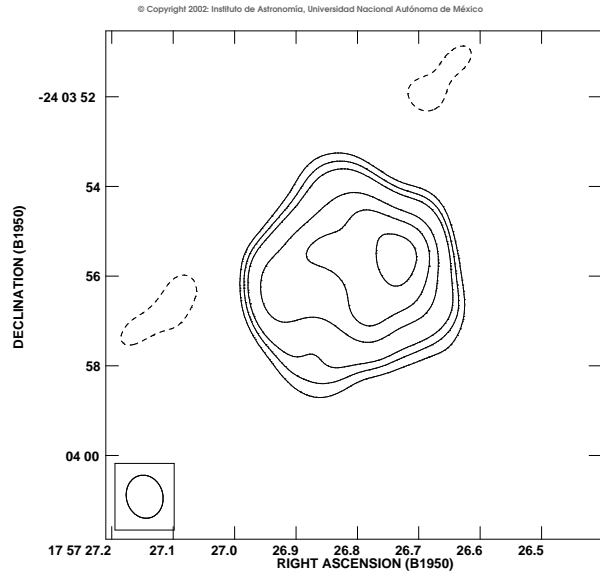


Fig. 5. VLA continuum contour map of G5.89–0.39 at 3.6 cm, made with natural weighting and a (u, v) taper of 200 k λ . Contour levels are $-3, 3, 4, 5, 6, 8, 10,$ and 12 times 11 mJy/beam, the rms noise of the map. The half power contour of the beam, $0''.97 \times 0''.81$, with $PA = 14^\circ$, is shown in the bottom left corner.

with the suggestion of Gaume et al. (1994) that the continuum emission from this source originates in an ionized stellar wind, since in this case a much wider line would be expected.

Finally, in Figure 4 we show the H92 α line emission for different radial velocities. The images clearly show the velocity gradient first seen by Garay et al. (1986), with the redshifted line emission coming from the southern half of the cometary and the blueshifted emission coming from the northern half.

3.2. G5.89–0.39

A 3.6 cm map of this region made from the continuum channel is shown in Figure 5. In Figure 6 we show grayscale images of the continuum, line, and line-to-continuum ratio of G5.89–0.39. The line emission is not detected over the entire nebula, but mostly toward the E and W edges.

The integrated line-to-continuum ratio goes from values ≤ 1 km s $^{-1}$ at the center of the nebula to 3–4 km s $^{-1}$ at the E and W edges. From the discussion given for G34.26+0.15, we believe that this result implies that the center of the nebula is optically thick in the continuum, with $\tau_c \geq 2$, while the edges are optically thin. This result is consistent with the value of the average opacity, $\tau_c(8.3 \text{ GHz}) \simeq 1.9$, derived from the analysis of Gómez et al. (1991). A sim-

ple model to explain the continuum and line emission can be made, following the suggestion of Zijlstra et al. (1990) that the ionized core of G5.89–0.39 has a disk-like morphology that is seen approximately edge-on.

In Figure 7 we show a cut made approximately in the E-W direction along the center of the nebula for the continuum, line, and line-to-continuum ratio. The cut was centered at $\alpha(1950) = 17^{\text{h}}57^{\text{m}}26^{\text{s}}.77$; $\delta(1950) = -24^\circ03'56''.6$ with a position angle of -95° . In the right-hand side of the same Fig. 7 we show the results from a simple LTE model made assuming that the disk has a cavity in its center, with radius of 42% of the total radius, and with a continuum optical depth of $\tau_c = 1.2$ for a line-of-sight along the center of the disk. We further assume that the ionized gas has an electron temperature of $T_e = 7000$ K. We modeled the expected emission using the transfer equation in the continuum as well as in the line emission, the former with a continuum optical depth as defined above, and the latter with a line optical depth $\tau_\ell \sim 0.84\tau_c$ (Dupree & Goldberg 1970) and a line width velocity of 70 km s $^{-1}$. Finally the results were convolved with a Gaussian beam of FWHM $\sim 0''.8$. As noted above, the results obtained are shown on the right part of Fig. 7. As can be seen from the figure, the agreement between the observations and our simple model is reasonable.

Zijlstra et al. (1990) found that the H76 α emission from the eastern edge peaked at $v_{\text{LSR}} \simeq 10$ km s $^{-1}$, while that from the western edge peaked at $v_{\text{LSR}} \simeq 30$ km s $^{-1}$ and suggested that this may imply rotation. The H92 α spectra of the eastern and western edges, shown in Figure 8, suggest a more complex situation. Toward the eastern edge we detect a single feature with a peak flux density of $S_\ell = 1.6 \pm 0.2$ mJy, a full width at half maximum of $\Delta v = 95 \pm 14$ km s $^{-1}$, and a radial velocity with respect to the local standard of rest of $v_{\text{LSR}} = 12 \pm 5$ km s $^{-1}$. This velocity component is consistent with the result of Zijlstra et al. (1990). However, toward the western edge we detect two features, one has $S_\ell = 2.0 \pm 0.2$ mJy, $\Delta v = 71 \pm 7$ km s $^{-1}$, and $v_{\text{LSR}} = -46 \pm 3$ km s $^{-1}$, while the other has $S_\ell = 1.2 \pm 0.2$ mJy, $\Delta v = 51 \pm 10$ km s $^{-1}$, and $v_{\text{LSR}} = 67 \pm 4$ km s $^{-1}$. This line emission appears to suggest more complex kinematics than that reported by Zijlstra et al. (1990) and we tentatively attribute the difference to the considerable optical depth of the source at 8.3 GHz or to peculiar kinematics. Zijlstra et al. (1990) attributed the observed velocity gradients to rotation, while our results suggest a less ordered model.

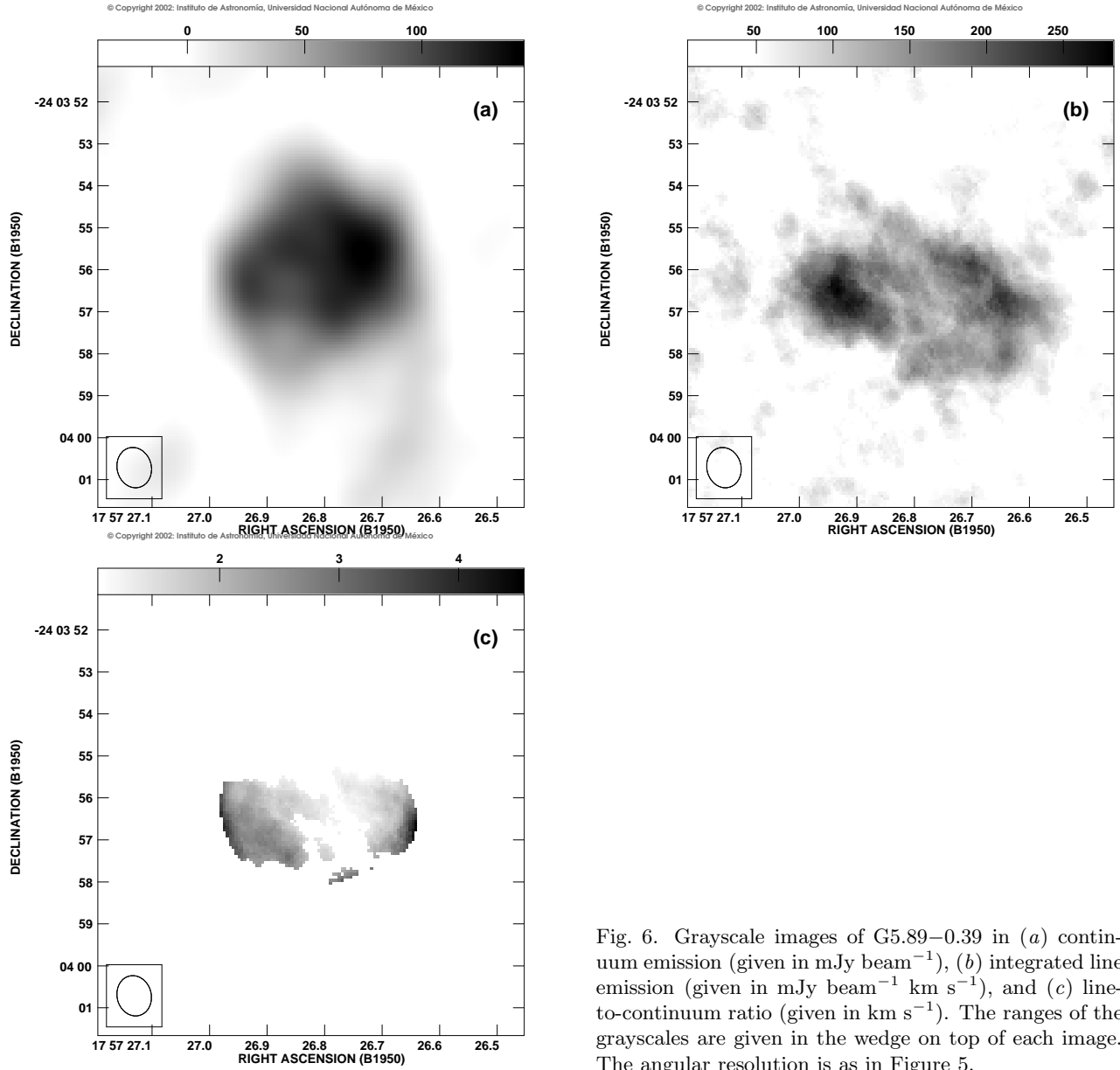


Fig. 6. Grayscale images of G5.89–0.39 in (a) continuum emission (given in mJy beam^{-1}), (b) integrated line emission (given in $\text{mJy beam}^{-1} \text{ km s}^{-1}$), and (c) line-to-continuum ratio (given in km s^{-1}). The ranges of the grayscales are given in the wedge on top of each image. The angular resolution is as in Figure 5.

4. CONCLUSIONS

Using the VLA, we observed 8.3 GHz continuum and H92 α radio recombination line toward the compact H II regions G34.26+0.15 and G5.89–0.39. Both sources have considerable optical depth at this wavelength and we discussed the continuum opacity variations across the face of the H II regions.

We detected for the first time radio recombination line emission from the ultracompact component A in G34.26+0.15. This detection is puzzling, since the region is optically thick in the continuum at the observed frequency and a much weaker line was expected.

We modeled adequately the continuum and integrated line emissions in G5.89–0.39 in terms of a disk-like structure such as the one proposed by Zijlstra et al. (1990). The velocity gradient in this source is complex and requires more than rotation to be explained.

We thank Paul Ho and Miller Goss for their valuable comments. We acknowledge the continuous economic support from DGAPA, UNAM, and CONACyT, México.

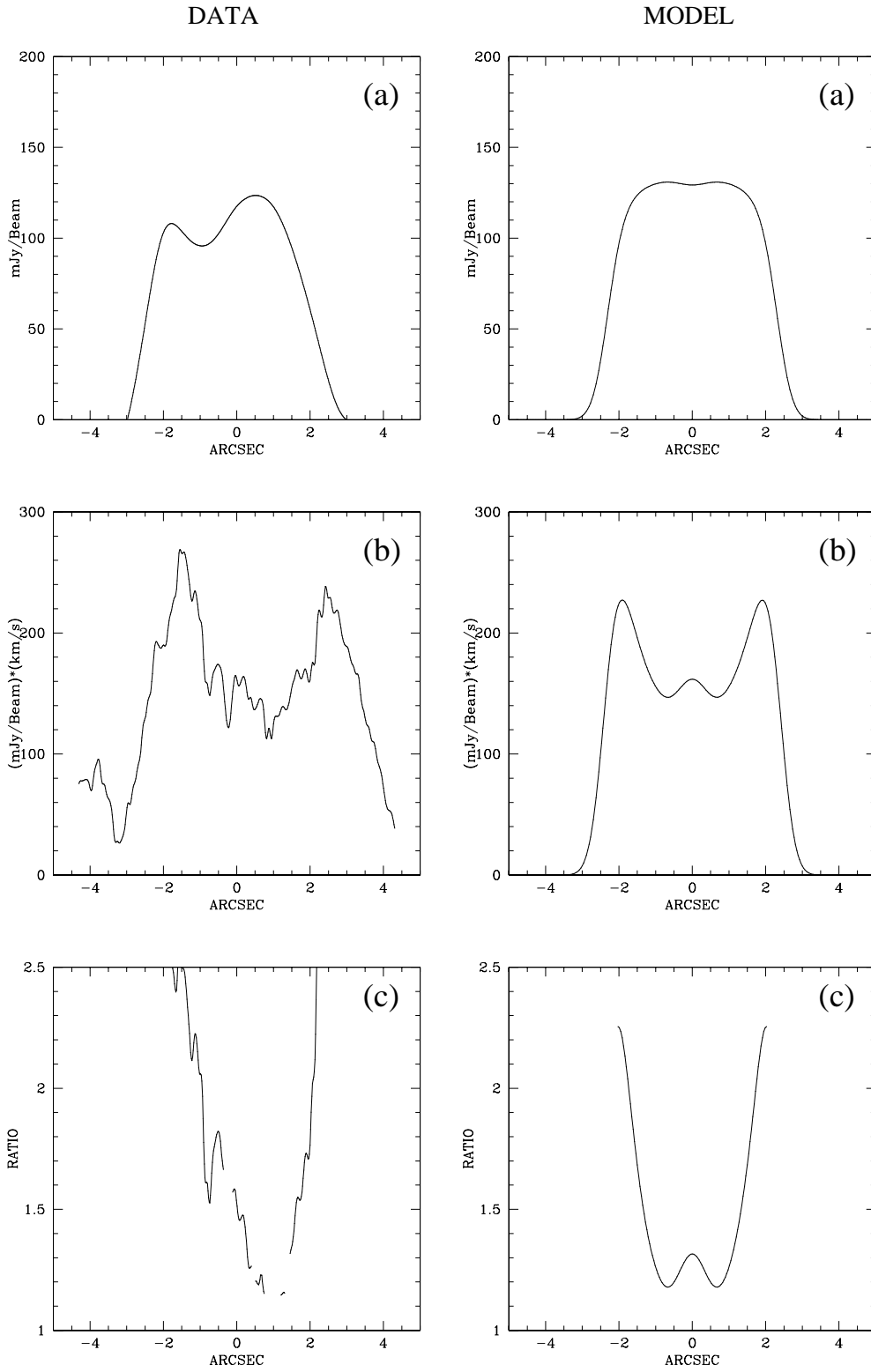


Fig. 7. Left: Slices of the source G5.89–0.39, in continuum (a), line integrated emission (b), and line-to-continuum ratio (c). Right: Cuts from the model described in the text for the same parameters of the left side of the figure.

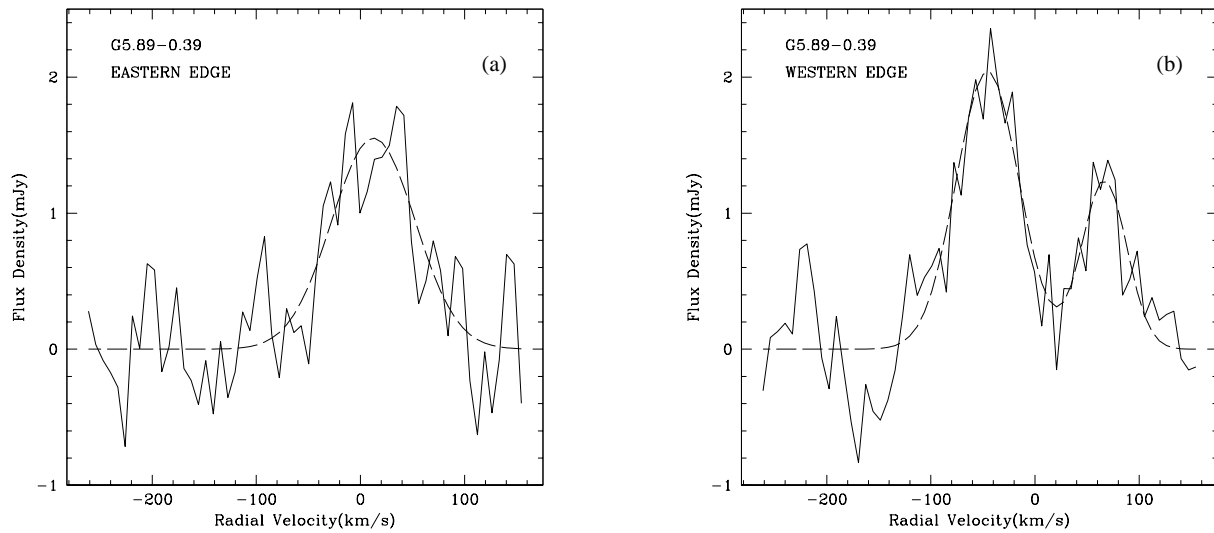


Fig. 8. (a) H92 α spectra from the eastern edge and (b) from the western edge of G5.89-0.39. The dashed line indicates the least-squares fit to the data.

REFERENCES

- Acord, J. M., Walmsley, C. M., & Churchwell, E. 1997, *ApJ*, 475, 693
- Afflerbach, A., Churchwell, E., Acord, J. M., Hofner, P., Kurtz, S., & Depree, C. G. 1996, *ApJS*, 106, 423
- Akeson, R. L., & Carlstrom, J. E. 1996, *ApJ*, 470, 528
- Andersson, M., & Garay, G. 1986, *A&A*, 167, L1
- Benson, J., & Johnston, K. 1984, *ApJ*, 277, 181
- Campbell, M. F., Garland, C. A., Deutsch, L. K., Hora, J. L., Fazio, G. G., Dayal, A., & Hoffmann, W. F. 2000, *ApJ*, 536, 816
- Carral, P., & Welch, W. J. 1992, *ApJ*, 385, 244
- Cesaroni, R., Walmsley, C. M., Kömpe, C., & Churchwell, E. 1991, *A&A*, 252, 278
- Downes, D., Wilson, T. L., Bieging, J., & Wink, J. 1980, *A&AS*, 40, 379
- Dupree, A. K., & Goldberg, L. 1970, *ARA&A*, 8, 231
- Fey, A. L., Gaume, R. A., Nedoluha, G. E., & Claussen, M. J. 1994, *ApJ*, 435, 738
- Garay, G., & Lizano, S. 1999, *PASP*, 111, 1049
- Garay, G., Lizano, S., & Gómez, Y. 1994, *ApJ*, 429, 268
- Garay, G., Reid, M. J., & Moran, J. M. 1985, *ApJ*, 289, 681
- Garay, G., & Rodríguez, L. F. 1990, *ApJ*, 362, 191
- Garay, G., Rodríguez, L. F., & van Gorkom, J. H. 1986, *ApJ*, 309, 553
- Gaume, R. A., Fey, A. L., & Claussen, M. J. 1994, *ApJ*, 432, 648
- Gaume, R. A., & Mutel, R. L. 1987, *ApJS*, 65, 193
- Gómez, Y., Rodríguez, L. F., Garay, G., & Moran, J. M. 1991, *ApJ*, 377, 519
- Gómez, Y., Rodríguez-Rico, C. A., Rodríguez, L. F., & Garay, G. 2000, *RevMexAA*, 36, 161
- Harvey, P. M., & Forveille, T. 1988, *A&A*, 107, L19
- Hatchell, J., Fuller, G. A., & Millar, T. J. 2001, *A&A*, 372, 281
- Heaton, B. D., Matthews, N., Little, L. T., & Dent, W. R. F. 1985, *MNRAS*, 217, 485
- Hofner, P., & Churchwell, E. 1996, *A&AS*, 120, 283
- Keto, E., Ho, P. T. P., & Reid, M. J. 1987, *ApJ*, 323, 117
- Kuchar, T. A., & Bania, T. M. 1994, *ApJ*, 436, 117
- Kurtz, S., Churchwell, E., & Wood, D. O. S. 1994, *ApJS*, 91, 659
- Reid, M. J., & Ho, P. T. P. 1985, *ApJ*, 288, L17
- Turner, B. E., Balick, B., Cudaback, D. D., Heiles, C., & Boyle, R. J. 1974, *ApJ*, 194, 279
- Watt, S., & Mundy, L. G. 1999, *ApJS*, 125, 143
- Wood, D. O. S., & Churchwell, E. 1989, *ApJS*, 69, 835
- Zheng, X., Reid, M. J., & Moran, J. M. 2000, *A&A*, 357, L37
- Zijlstra, A. A., Pottasch, S. R., Engels, D., Roelfsema, P. R., Te-Lintel Hekkert, P., & Umana, G. 1990, *MNRAS*, 246, 217.

Yolanda Gómez and Luis F. Rodríguez: Instituto de Astronomía, UNAM, Apartado Postal 3-72, 58090 Morelia, Michoacán, México (y. gomez, l.rodriguez@astrosmo.unam.mx).

Carlos A. Rodríguez-Rico: National Radio Astronomy Observatory, P.O. Box 0, Socorro, NM 87801, USA (crodrigu@nrao.edu).